An Evaluation of Lesion Detectability with Cone-Beam, Fanbeam and Parallel-Beam Collimation in SPECT by Continuous ROC Study

Jianying Li, Ronald J. Jaszczak, Timothy G. Turkington, Charles E. Metz, Dave R. Gilland, Kim L. Greer and R. Edward Coleman

Department of Radiology, Duke University Medical Center, Durham, North Carolina; and Department of Radiology, The University of Chicago, Chicago, Illinois

To evaluate lesion detectability for clinical evaluation of cone-beam (CB), fanbeam (FB) and parallel-beam (PB) collimator sensitivity, experimentally acquired phantom data were used to assess the advantage of CB collimation over conventional collimation. **Methods:** Lesion detectability with CB, FB and PB collimation in SPECT was compared using a three-dimensional brain phantom and continuous receiver operating characteristic (CROC) analysis. A simulated cold lesion was located near the posterior portion of the thalamus. High count density scans of this phantom were acquired with CB, FB and PB collimators with similar resolution. These projections were scaled to count levels which reflected the measured sensitivities of the three collimators. Computer-generated Poisson noise was added to the projections to produce uncorrelated data sets. Images were reconstructed using a filtered backprojection algorithm. All reconstructions used a Hann filter with multiplicative attenuation correction. Each of seven trained observers viewed 288 sets of images and indicated the certainty of perceiving a cold lesion at a specified location by a rating of 0–100. Each image set contained four adjacent slices centered on the lesion to minimize partial volume effects. The program LABROC4 was used to fit CROC curves to individual observers' ratings. A t-test for paired data was performed on the individual areas. **Results:** The average areas (standard deviations) under CROC curves for CB, FB and PB were 0.89 (0.03), 0.83 (0.05) and 0.76 (0.04), respectively. The differences of the areas were statistically significant with all two-tailed p values < 0.02. **Conclusion:** These results demonstrate that cold lesions in the posterior portion of the thalamus are best detected by images obtained using CB followed by FB and PB collimation.

Key Words: cone-beam collimation; fanbeam collimation; parallel-beam collimation; SPECT; ROC study cold lesions

J Nucl Med 1994; 35:135–140

Single-photon emission computed tomography (SPECT) using cone-beam (CB) collimation increases the number of detected photons compared with conventional acquisition geometries (*1–3*). However, the advantage of CB collimation over conventional collimation in terms of lesion detectability has yet to be evaluated. The evaluation of lesion detectability is a prerequisite for clinical application of CB SPECT. In this paper, we compare lesion detectability using CB, fanbeam (FB) and parallel-beam (PB) collimation using the Hoffman three-dimensional brain phantom and continuous receiver operating characteristic (CROC) analysis.

Many factors, such as resolution and sensitivity of the detection system, reconstruction algorithm, lesion size and lesion location, affect the lesion detectability. In this study, we investigate the effect of collimator sensitivity on lesion detectability using experimentally acquired phantom data. CB, FB and PB collimators having similar resolution characteristics were used to minimize the possible detectability variations because of the different resolutions of different collimators (*4*). The lesion size was chosen, in combination with the count level, to provide the appropriate degree of detection difficulty and to minimize the potential partial volume effect while remaining within the specifications of clinical abnormality.

Images obtained using CB, FB and PB collimation were reconstructed using a filtered backprojection (FBP) algorithm. With FBP reconstruction, image quality is greatly affected by the choice of filter and cut-off frequency. For converging beam collimation (CB, FB), the Nyquist frequency sampled changes for objects at different distances from the detector surface due to the magnification. The root mean square (rms) noise of FBP reconstructed images is proportional to the integral of the square of the spatial frequency filter function (*5*). The primary objective of this study is to evaluate the effect of collimator sensitivity on lesion detectability. We therefore used a Hann filter with the same cutoff frequency for the plane at the distance of the radius-of-rotation (ROR) from the detector surface for

Received Apr. 21, 1993; revision accepted Aug. 2, 1993.
For correspondence and reprints contact: Jianying Li, PhD, Box 3949, Dept. of Radiology, Duke University Medical Center, Durham, NC 27710.

TABLE 1
Dimensions of Collimators

Collimator	Hole shape	Focal length (cm)	Collimator thickness (cm)	Effective hole size (cm)	Septal thickness (cm)
Cone-beam	Hexagonal	50	4.06	0.190	0.025
Parallel-hole	Square	—	2.46	0.115	0.015
Fanbeam	Triangle	58	5.08	0.264	0.025

all reconstructions to obtain equal areas under the filter curves for that plane. The cutoff frequency was equal to the Nyquist frequency of PB collimation.

Quantitative evaluation of alternative imaging systems using receiver operating characteristic (ROC) analysis is widely recognized as an appropriate methodology in the field of image evaluation (*6–8*). Most of the ROC studies conducted in medical imaging use a discrete rating scale with five or six categories. However, successful use of discrete rating scales requires the readers to employ a well-distributed scoring pattern to allow a smooth ROC curve to be fit to the data (*9–10*). In extreme cases, an ROC estimated from discrete rating data may depend strongly on the way in which an observer distributes his or her responses across the scale, even when curve fitting is possible (*9*). Recently, the use of a continuous rating scale in ROC studies was proposed (*11,12*) to avoid these extreme situations. ROC analysis using a continuous rating scale has the potential advantages of approximating clinical reporting more closely and increasing the likelihood of successful ROC curve fitting compared with the use of a discrete rating scale (*12*). In this study, the continuous rating scale method was used.

METHODS

Data Preparation

A Hoffman three-dimensional brain phantom (Data Spectrum Corp., Hillsborough, NC) was used to acquire data for the CROC study. The brain phantom contained 19 slices, each of which was 6.3 mm thick. The radius of these slices was 9.5 cm. The brain phantom was filled with 27 mCi of ^{99m}Tc-pertechnetate in water. Two small pieces of rubber (~0.5 cm^3) were placed side by side into two adjacent slices near the posterior portion of the thalamus to simulate a cold lesion. The rubber pieces were separately checked to be sure that they did not absorb the radiopharmaceutical used in the phantoms. High count density and relatively low noise scans (>500 Mcts) of this three-dimensional brain phantom with and without the lesion were acquired with CB, FB and PB collimators having similar resolution characteristics which was about 10 mm at 15 cm from the collimator. All collimators had a circular field of view (FOV) and a diameter of 40 cm and were placed parallel to the axis of rotation. The CB collimator was a high-resolution collimator with a 50-cm focal length. The PB collimator was a low-energy, high-resolution (LEHR) collimator, which was also used for clinical studies. The collimator specifications for the CB and PB collimators have been reported (*2*). The FB collimator was a prototype collimator (*13*) with a 58-cm focal length and had similar resolution characteristics with CB and PB collimators. Table 1 summarizes the dimensions of the three collimators. The reason to choose CB, FB and PB collimators with similar resolution characteristics was to minimize the possible detectability variations caused by different resolutions of different collimators (*4*). The three-dimensional brain phantom was centered on the axis of rotation, and the radius of rotation was 14 cm measured to the patient side of the collimator for all the phantom scans. Experiments were performed on a single-camera SPECT system (Siemens Orbiter, Model #ZLC7500, Siemens Medical Systems, Hoffman Estates, IL). All the projections consisted of 128 angular views over 360°. Each view was a 128-by-128 array. The angular and linear sampling intervals were equal to 2.8 degrees and 3.1 mm at the detector surface, respectively. Each projection was acquired for approximately 150 sec/stop. The total acquisition time for each brain phantom scan was about 5 hr. The counting rate using a CB collimator was less than 38,000 counts/sec, and the maximum electronic deadtime was <8%. The electronic deadtime variation between the first angular view and the last angular view was <4%. After the acquisition, all projections were corrected for the decay of the radionuclide on an angular view-by-angular view basis.

SPECT acquisition using converging beam geometries (CB and FB) can result in two important kinds of misalignments; mechanical shift and electronic shift (*14,15*). Mechanical shift is the displacement of the mechanical center-of-rotation off the midline of a CB (FB) geometry. Mechanical shift happens in object space, and hence the translations of the projections caused by this shift are depth-dependent. On the other hand, electronic shift or electronic centering misalignment does not depend on the object or the detection angle and causes the projections to have a collective translation. In order to obtain high quality images, it is very important to determine these shifts and make corrections. Thus, the detection system was carefully monitored in this study. A point source scan over 360° was taken before each phantom scan. The system's electronic shift and mechanical shift were determined using the centroid of the projected point source based on the Marquardt nonlinear fitting algorithm (*15*). The determined electronic shift was then used to pre-correct the projections and the mechanical shift was incorporated into the reconstruction algorithm (*16*).

Additional scans of the uniform cylinder which held the brain phantom were taken using CB, FB and PB collimators for attenuation correction. A specially designed holder was used to ensure that the cylinder with and without the brain phantom was placed at the same position. The projections of the uniform cylinder were also corrected for the decay of the radionuclide and were used to calculate the relative sensitivity of CB, FB and PB collimators. For the three-dimensional brain phantom and the acquisition geometries used, the relative sensitivities of CB, FB and PB collimators were 1.70, 1.38 and 1.00, respectively.

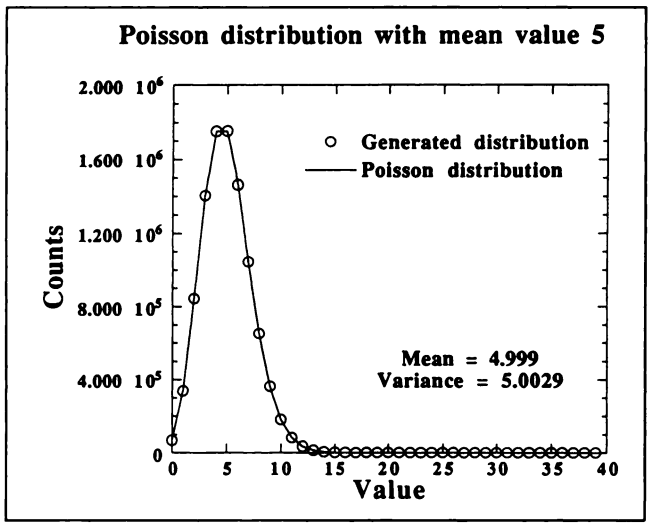

FIGURE 1. Comparison between the theoretical and generated Poisson distributions.

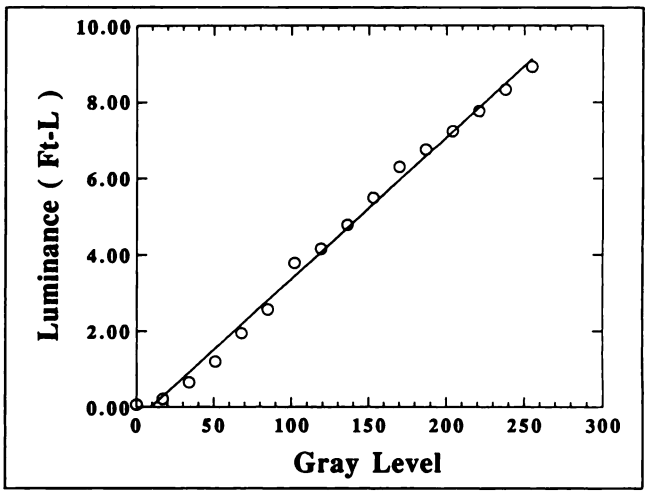

FIGURE 2. Measurement of luminance versus gray level. The dots are measured points and the line is the fit to the points.

The electronic shift-corrected projections were scaled to desired count levels which reflected the measured sensitivity ratio of the three collimators. The count level was defined as the total counts for all angular views per image slice. For the PB collimator, the count level was about 40,000 counts/slice. The count level was chosen based on pilot studies so that the average areas under ROC curves were in the range of 0.75–0.85. This count level was similar to count levels obtained for clinical scans. Computer generated Poisson noise with different seeds was added to the projections to produce 288 uncorrelated data sets that were reconstructed for the CROC study. The Poisson noise generator was tested using 10^7 samples of a distribution with mean value of 5.0. The generated distribution had a mean value of 4.9999 and variance of 5.0029. Figure 1 compares the generated data with a Poisson distribution.

Image Reconstruction

A modified filtered backprojection (FBP) algorithm which corrected mechanical shift was used to reconstruct images obtained using CB, FB and PB collimation of the same image size (*17*). For PB data, a sufficiently large focal length (10000 cm) was used. To reduce the computational burden, all projections were reduced to 64 × 64 × 128 angular views prior to reconstruction. The reconstruction matrix was 64^3, which corresponded to a 6.3-mm pixel size and slice thickness. All reconstructions used a Hann filter with the same cutoff frequency which was 0.79 cycle/cm to obtain equal areas under the filter curves. The mechanical shift correction was done by incorporating the mechanical shift into the algorithm (*16*). The images of a uniform cylinder were reconstructed using the same protocol. Assuming that the reconstructed images of a uniform cylinder should be uniform, we generated multiplicative matrices on a slice-by-slice basis for brain images of CB, FB and PB collimators. The images of the brain phantom were multiplied by these multiplicative factors to correct for attenuation and residual detector nonuniformity. We generated 96 image sets for each of three modalities, half with the lesion and half without. The 48 images without the lesion were generated using scans of the normal three-dimensional Hoffman brain phantom.

Image Display

The three-dimensional brain images for the CROC study were displayed in gray-scale on a 19-inch color monitor capable of 256 gray levels (Stardent GS1000 monitor, Stellar Computer Inc., Newton, MA). The luminance range of the monitor was measured with a digital photometer (Minolta Auto-Spot II, Minolta Ltd., Japan). A linear response between luminance and gray level pixel value was found. The luminance was 0.06 foot-lamberts for a display driving intensity of zero and 8.9 foot-lamberts for driving intensity of 255. Figure 2 shows the relation between luminance and gray level.

Each image set contained four adjacent slices centered on the lesion to minimize partial volume effects. The original reconstructions were linearly interpolated to 512 × 512 for display, which corresponded to a displayed image size of 13.5 × 13.5 cm. The negative values in the images were truncated to zero for display purposes. The potential lesion locations were indicated by using cross hairs, which could be clicked on and off with a mouse button. An example of the image display is shown in Figure 3.

Global linear min-max windowing was used in the image display in order to ensure proper image contrast (*18*). All images were displayed using the entire luminance range of the monitor

FIGURE 3. An example of image display. Each image contains four adjacent slices centered on the lesion. The potential lesion locations are indicated by using cross hairs.

with the window minimum set to zero pixel intensity. In order to avoid the problem of reduced displayed contrast in an image that had one or a few extremely high intensity pixels as a result of noise, the window maximum was not set to the maximum pixel intensity on an image-by-image basis. Instead, a window maximum for images in each modality was determined from the images reconstructed from noiseless projections with the same mean pixel value in that modality. The window maximum was set to 1.1 times the maximum intensity of noiseless images.

The ROC study employed seven observers: three board certified nuclear medicine physicians, three radiological physicists experienced in ROC studies, and a graduate student in biomedical engineering. Each observer viewed a total of 96 independent image sets for each of the three modalities and indicated the certainty with which the observer perceived a cold lesion at a specified location. A continuous rating method (0–100) was used. Images were considered independent because they were obtained from different projection data. In order to reduce reading order effects, the image presentation technique suggested by Metz (*9*) was used. The ROC study was divided into two sessions with 48 image sets for each modality, and observers finished one session for each modality before starting the complementary session. In each session the image was further split into three subsets and various modality-subset combinations were sequenced so that each image was read first in each modality by two observers or three observers (in one case), and yet no observer used the same sequence.

The ROC study was conducted in a controlled environment. The contrast and brightness of the monitor were fixed and were the same for all observers. The observers were trained prior to each phase of the ROC study. The training sessions consisted of 20 images for each of the modalities and for each of the subsets. Training images were also independent and none of them were used in the actual ROC study. After each response during the training session, the nearly noiseless image was displayed next to the test image, thereby indicating the true state of the image.

ROC Analysis

The program LABROC4 (*19*) was used to fit CROC curves to individual observers' rating data and to calculate the parameters "a" and "b" and to compute the area under the CROC curve (A_z). LABROC4 is a newly developed curve-fitting program for continuously distributed data that preserves all of the information in the raw data that is relevant to the ROC. The parameter A_z is equivalent to the percent correct in a two-alternative-forced-choice experiment (*20*) and was used as the figure-of-merit for observer performance. LABROC4 produces the estimates of the ROC parameters "a" and "b," the area under fitted curve A_z and its standard deviation σ for each of the three modalities. Using the areas and their standard deviations, we calculated the two-tailed p-values to test the significance of the difference between two A_z scores within individual observers. The null hypothesis of this test was that the resulting area difference between two sets of rating data arose from CROC curves was equal to zero. Student's t-tests for paired data were also performed on the A_z values averaged across observers. The differences of the A_z values between two modalities across observers were averaged, and a standard deviation of these differences were calculated. Based on the averaged difference in A_z and its standard deviation, a p value was obtained.

RESULTS

To describe the overall performance of the group of observers, the resulting parameters "a" and "b" for each of the three modalities were averaged across seven observers to produce an averaged ROC. Figure 4 compares the averaged ROC curves for CB, FB and PB collimation. Also shown in Figure 4 are the areas under the averaged ROC curves. They were calculated using the averaged parameters "a" and "b."

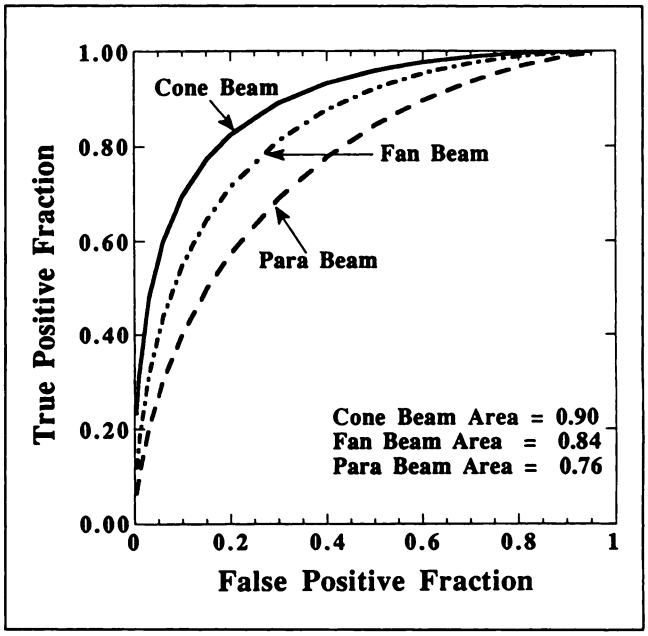

FIGURE 4. Averaged ROC curves for cone-beam, fanbeam and parallel-beam collimation. Also listed in the figure are the averaged areas under the ROC curves and the p-values from the paired t-test.

Table 2 lists the areas and their standard deviations for the three modalities calculated using program LABROC4. These areas were also averaged and are listed in the last row. These averaged areas were very close to those obtained by using averaged parameters "a" and "b." The two-tailed p values of the statistical test of the difference between two A_z scores within individual observers were calculated, and they are listed in the last three columns for CB versus PB, CB versus FB and FB versus PB, respectively. The results indicate that, in terms of lesion detectability, CB collimation was significantly better than PB and FB collimation (except in one case where the FB area was only marginally greater than the CB area). FB collimation was also judged better than PB collimation, although the differences were not as great as CB versus PB or CB versus FB.

Greater statistical power can be achieved by testing the significance of A_z differences averaged across observers, although this comparison ignores case-sample variation (*9*). Table 3 lists the Student's t-test of the significance of the difference in A_z averaged across observers. The null hypothesis was that the population mean of the resulting difference between two modalities was equal to zero. The calculated probabilities (two-tailed p values) that the observed difference could have arisen from the assumed distribution, given that the null hypothesis was true, were all <0.02. These small p values strongly rejected the null

TABLE 2
Individual Results of ROC Study Using Continuous Rating Scale for Cone-Beam, Fanbeam and Parallel-Beam Collimation

Observer	A_{CB}*	σ_{CB}†	A_{FB}*	σ_{FB}†	A_{PB}*	σ_{PB}†	p_{CP}‡	p_{CF}‡	p_{FP}‡
1	0.92	0.027	0.85	0.039	0.82	0.043	0.05	0.11	0.62
2	0.91	0.032	0.85	0.040	0.78	0.046	0.03	0.27	0.25
3	0.91	0.029	0.80	0.044	0.73	0.051	0.005	0.04	0.35
4	0.90	0.031	0.84	0.040	0.82	0.043	0.10	0.24	0.64
5	0.89	0.034	0.93	0.025	0.74	0.050	0.02	0.32	0.001
6	0.87	0.037	0.79	0.046	0.75	0.049	0.06	0.17	0.52
7	0.84	0.040	0.76	0.049	0.70	0.052	0.04	0.16	0.40
Average	0.89	0.03	0.83	0.05	0.76	0.04			

*A_{CB}, A_{FB} and A_{PB} are the areas under CB, FB and PB ROC curves, respectively.
†σ_{CB}, σ_{FB} and σ_{PB} are the standard deviations of the areas A_{CB}, A_{FB} and A_{PB}, respectively.
‡p_{CP}, p_{CF} and p_{FP} are the two-tailed p-values comparing areas under ROC curves for CB versus PB, CB versus FB and FB versus PB, respectively.

hypothesis, indicating that lesions near the thalamus were best detected by images obtained using CB followed by FB and PB collimation.

DISCUSSION

The lesion detectability using CB, FB and PB collimation and SPECT was compared using the Hoffman three-dimensional brain phantom and ROC methodology. The effect of the relative sensitivities of CB, FB and PB collimators on the lesion detectability was evaluated. Cold lesions located in the posterior portion of the thalamus were best detected on images obtained using CB followed by FB and PB collimation. Many factors, such as reconstruction algorithms or lesion locations, may affect the relative lesion detectability, and the results of this study are not intended to be generalized outside this context.

In this study, we first acquired high count density, relatively low noise scans of the three-dimensional brain phantom and then added Poisson noise to generate noisy data sets. Because of the long scan time used, the camera electronic deadtime varied during the scan. This may cause the data to be inconsistent. However, we found that the electronic deadtime variations were small (<4%) and the artifacts that might be caused by the data inconsistency should be negligibly small compared with those caused by the noise.

TABLE 3
Averaged Results of ROC Study Using Continuous Rating Scale for Cone-Beam, Fanbeam and Parallel-Beam Collimation

DA_{CP}*	p_{CP}†	DA_{CF}*	p_{CF}†	DA_{FP}*	p_{FP}†
0.13	0.001	0.06	<0.02	0.07	<0.02

*DA_{CP}, DA_{CF} and DA_{FP} are the area differences comparing areas under averaged ROC curves for CB versus PB, CB versus FB and FB versus PB, respectively.
†p_{CP}, p_{CF} and p_{FP} are the two-tailed p values comparing areas under averaged ROC curves for CB versus PB, CB versus FB and FB versus PB, respectively.

Since the purpose of this study was to evaluate the relative performance of CB, FB and PB collimators, a single-headed camera was used and count levels and lesion size were chosen so that the average areas under ROC curves were in the range of 0.75–0.85. In clinical situations, two- or three-headed camera systems are now also widely used. The use of a three-headed camera, equipped with the same collimators used in this study should increase cold lesion detectability (in terms of area under the ROC curve) by about 20%. However, the use of two- or three-headed camera systems should not affect the relative performance of CB, FB and PB collimators.

If the two modalities have similar resolution characteristics and the lesion is centrally located in the uniform attenuation media, the lesion detectability ratio between two modalities may be estimated based on a signal-to-noise analysis. This estimation is based on the assumptions that the decision variables are Gaussian and the reconstruction method is linear. Using the sensitivity ratios measured for CB, FB and PB collimation for brain imaging and assuming that the area under FB ROC curve is 0.83, the areas under CB and PB ROC curves are 0.86 and 0.79, respectively. This prediction agrees with the experimental results fairly well. The difference between the predicted and observed values may be because the lesion is located off-center and attenuation and scatter are different at different angles for the three different collimators.

The choice of the cutoff frequency for image reconstruction is an important issue in this study. In PB geometry, the highest frequency sampled is determined by the pixel size. This highest frequency or Nyquist frequency (N_f(PB)) is equal to $1/(2\Delta t)$, where Δt is the pixel size. In CB or other converging beam geometries, the highest frequency that can be sampled is no longer a constant because of the magnification. The highest frequency that can be sampled changes for objects at different distances from the collimator and can be expressed as $N_f(CB) = N_f(PB) * fm$, where fm is the magnification factor. Since fm is ≥ 1, N_f(CB) is always larger or equal to N_f(PB). For a plane with distance

equal to the radius-of-rotation from the collimator in CB geometry, N_f(CB) becomes N_f(PB) * F/S, where F is the focal length of CB geometry and S is the distance between the focal point and the center-of-rotation. Therefore, if we use N_f(CB) (N_f(FB)) as a cutoff frequency for CB (FB) geometry, we actually allow more of the higher frequencies to pass through. The root mean square (rms) noise level in reconstructed images is proportional to the square root of the algorithm filter factor (FF), where FF is the integral of the square of the spatial frequency filter function (*5*). A higher cutoff frequency means a larger FF, which in turn means more noise. Since the primary objective of this study was to investigate the effect of collimator sensitivity on the lesion detectability, the influence of the filter on lesion detectability should be minimized. In this study we chose to use the same cutoff frequency, which is equal to the Nyquist frequency in PB geometry, for the plane with distance of the ROR from the collimator for all reconstructions. This choice ensures the same FF for all reconstructed images in the plane with a distance equal to the ROR from the collimator. Although in CB or FB geometries a smaller FF is obtained for planes with a distance shorter than the ROR and a larger FF is obtained for planes with a distance longer than the ROR, the deviations of FF tend to cancel out since the detector rotates around the axis of rotation.

CB SPECT can increase the number of detected photons compared with conventional PB collimation. However, due to the lack of an appropriate filter in the axial direction for the FBP algorithm and insufficient sampling of the CB geometry, artifacts may result for sources located further away from the central plane (*21–23*). In addition, it is more appropriate to use tilted CB geometry in a clinical situation to clear the patient's shoulders. The use of tilted CB geometry introduces more axial blurring for the structure near the vertex of the brain which is closer to the CB collimator. It is not clear how the blurring may influence the relative lesion detectability of CB collimation compared with PB and FB collimation which does not have an axial blurring problem. Further studies are required in order to establish a clear relationship between lesion detectability and detection/reconstruction modality. These studies may compare the lesion detectability with lesions located at different places, for example, near the vertex of the brain, and with different detection geometries, for example, tilted CB geometry or half-CB geometry (*1*). CB iterative reconstructions have been reported to improve image quality compared with the filtered backprojection reconstructions (*22*). The improvement is best demonstrated in the axial direction. However, this observation needs to be quantitatively evaluated using ROC methodology. The current version of a three-dimensional CB iterative reconstruction is computationally expensive. Due to the requirement of a large number of images in ROC studies, it is necessary to greatly reduce the computational time of a CB iterative reconstruction algorithm before a practical ROC study can be carried out.

ACKNOWLEDGMENTS

The authors thank Drs. J. Hoffman, V. Lowe, R. Reiman, H. Wang and Mr. S. Jang of the Department of Radiology at Duke University Medical Center for their participation in this study. This work was supported by PHS Grant R01-CA33541 awarded by the National Cancer Institute and in part by Grant DE-FG05-91ER60894 awarded by the Department of Energy.

REFERENCES

1. Jaszczak RJ, Floyd CE, Manglos SH, Greer KL, Coleman RE. Cone- beam collimation for SPECT: analysis, simulation and image reconstruction using filtered backprojection. *Med Phys* 1986;13:484–489.
2. Jaszczak RJ, Greer KL, Coleman RE. SPECT using a specially designed cone-beam collimator. *J Nucl Med* 1988;29:1398–1405.
3. Jaszczak RJ, Greer KL, Floyd CE, Manglos SH, Coleman RE. Imaging characteristics of a high resolution cone collimator. *IEEE Trans Nucl Sci* 1988;35:644–648.
4. Tsui BMW, Metz CE, Atkins FB, Starr SJ, Beck RN. A comparison of optimum detector spatial resolution in nuclear imaging based on statistical theory and on observer performance. *Phys Med Biol* 1978;23:654–676.
5. Jaszczak RJ, Coleman RE, Whitehead FR. Physical factors affecting quantitative measurements using camera-based single photon emission computed tomography (SPECT). *IEEE Trans Nucl Sci* 1981;28:69–80.
6. Metz CE. Basic principles of ROC analysis. *Semin Nucl Med* 1978;8:283–298.
7. Swets JA, Picket RM. Fundamentals of accuracy analysis. In: *Evaluation of diagnostic systems: methods from signal detection theory*. Academic Press; New York: 1982:15–45.
8. Metz CE. ROC methodology in radiological imaging. *Invest Radiol* 1986; 21:720–733.
9. Metz CE. Some practical issues of experimental design and data analysis in radiological ROC studies. *Invest Radiol* 1989;24:234–245.
10. Rockette HE, Gur D, Cooperstein LA, et al. Effect of two rating formats in multi-disease ROC study of chest images. *Invest Radiol* 1990;25:225–229.
11. Swets JA, Getty DJ, Pickett RM, D'Orsi CJ, Seltzer SE, McNeil BJ. Enhancing and evaluating diagnostic accuracy. *Med Decis Making* 1991;11:9–16.
12. Rockette HE, Gur D, Metz CE. The use of continuous and discrete confidence judgments in receiver operating characteristic studies of diagnostic imaging techniques. *Invest Radiol* 1992;27:169–172.
13. Jaszczak RJ, Chang LT, Murphy PH. Single-photon emission computed tomography using multi-slice fan beam collimators. *IEEE Trans Nucl Sci* 1979;26:610–618.
14. Jaszczak RJ, Greer KL, Coleman RE. SPECT system misalignment: comparison of phantom and patient images. In: Esser PD, ed., *Emission computed tomography: current trends*. New York: Society of Nuclear Medicine; 1983:57–70.
15. Li J, Jaszczak RJ, Wang H, Greer KL, Coleman RE. Determination of both mechanical and electronic shifts in cone-beam SPECT. *Phys Med Biol* 1993;38:743–754.
16. Li J, Jaszczak RJ, Wang H, Gullberg GT, Greer KL, Coleman RE. A cone-beam reconstruction algorithm with a displaced center-of-rotation. *Med Phys* 1993: in press.
17. Li J, Jaszczak RJ, Greer KL, Coleman RE, Cao Z, Tsui BMW. Direct cone-beam SPECT reconstruction with camera tilt. *Phys Med Biol* 1993;38:241–258.
18. Gilland DR, Tsui BMW, Metz CE, Jaszczak RJ, Perry JR. An evaluation of maximum likelihood-expectation maximization reconstruction for SPECT by ROC analysis. *J Nucl Med* 1992;33:451–457.
19. Metz CE, Shen JH, Herman BA. New methods for estimating a binomial ROC curve from continuously-distributed test results. Presented at the 1990 Joint Statistical Meetings of the American Statistical Society and the Biometric Society; Anaheim, CA, August 1990.
20. Green DM, Swets JA. *Signal detection theory and psychophysics*, revised edition. Huntington, New York: R.E. Krieger Publishing Co., 1974.
21. Zeng GL, Gullberg GT. A study of reconstruction artifacts in cone- beam tomography using filtered backprojection and iterative EM algorithms. *IEEE Trans Nucl Sci* 1990;37:759–765.
22. Jaszczak RJ, Li J, Wang H, Greer KL, Coleman RE. Three-dimensional SPECT reconstruction of combined cone-beam and parallel beam data. *Phys Med Biol* 1992;37:535–561.
23. Li J, Jaszczak RJ, Greer KL, Coleman RE. SPECT reconstruction of combined cone-beam and parallel hole collimation with experimental data. *IEEE Trans Nucl Sci* 1993;40:300–306.